Technical Note

Toe-Bearing Capacity of Precast Concrete Piles through Biogrouting Improvement

Yang Xiao, M.ASCE[1]; Armin W. Stuedlein, M.ASCE[2]; Zhengyu Pan[3]; Hanlong Liu, M.ASCE[4]; T. Matthew Evans, M.ASCE[5]; Xiang He[6]; Hai Lin[7]; Jian Chu[8]; and Leon A. van Paassen[9]

Abstract: This technical paper investigates the bearing performance of precast concrete piles embedded within calcareous sands with biogrouting at the pile toe. Loading tests of biogrout-improved and unimproved concrete model piles were conducted to evaluate the performance of biogrout to enhance the toe bearing capacity of precast concrete piles. The total bearing capacity of the precast concrete pile with a biogrouted toe was 4.4 times as large as that without biogrout. A series of index tests were performed using a penetrometer to estimate the spatial distribution of strength of biocemented sands below the pile toe. It was found that the average strength of the biocemented sand below the biogrouted pile toe gradually decreased with increasing vertical distance or lateral distance from the pile toe. The novel application of biocement to treat bearing sands following pile installation represents a promising method to increase pile capacity. **DOI: 10.1061/(ASCE)GT.1943-5606.0002404.**

Author keywords: Microbially-induced calcium carbonate precipitation (MICP); Biogrout; Toe-bearing capacity; Strength; Concrete pile.

Introduction

The mechanical characteristics of calcareous sand, as compared with those of silica sand or granitic sand, are characterized by its highly compressible and crushable response during loading (Coop 1990; Hyodo et al. 1996; Coop et al. 2004; Lade et al. 2009; Bandini and Coop 2011; Miao and Airey 2013; Xiao et al. 2019b; Yu 2019). Previous studies have extensively investigated the behavior of pile foundations in calcareous sediments, including their toe-bearing capacity (Murff 1987; Yasufuku and Hyde 1995; Yasufuku et al. 2001; Kuwajima et al. 2009; Zhang et al. 2013), shaft resistance (Lee and Poulos 1988; Lehane et al. 2012), lateral resistance (Dyson and Randolph 2001), and pile displacement (White and Bolton 2004; Mao et al. 2018). Low bearing capacity and large displacements are common for piles in calcareous sand foundations (Murff 1987; Yasufuku and Hyde 1995; Zhang et al. 2013). These characteristics are primarily attributed to particle crushing around the pile (Yasufuku et al. 2001; Coop et al. 2004). Grouted piles using cementitious grout have been used to improve the bearing capacity and deformation performance of deep foundations in calcareous sand (Lee and Poulos 1991; Spagnoli et al. 2015; Doherty et al. 2016). However, grouting techniques based on cement or chemical reagents result in additional energy consumption and environmental pollution (Lee and Poulos 1991; Doherty et al. 2016). In recent years, biogrouting using microbially-induced calcium carbonate precipitation (MICP) has attracted considerable attention because of its high efficacy, low viscosity coefficient, and environmental friendliness. In addition, this method provides a substantial increase in strength and dilatancy, and a substantial decrease in hydraulic conductivity (DeJong et al. 2010; van Paassen et al. 2010a; Chou et al. 2011; Al Qabany and Soga 2013; Burbank et al. 2013; Chu et al. 2013; Martinez et al. 2013; Montoya and Dejong 2013; Montoya et al. 2013; Montoya and DeJong 2015; O'Donnell and Kavazanjian 2015; Cheng and Shahin 2016; Li et al. 2016; Terzis et al. 2016; Cheng et al. 2017; Cheng and Shahin 2017; Cui et al. 2017; Jiang et al. 2017; Li et al. 2017; Gao et al. 2018; Xiao et al. 2018; Montoya et al. 2019; Xiao et al. 2019a). Urea hydrolysis is commonly used in MICP-treatment and involves the following reaction (Nemati and Voordouw 2003; DeJong et al. 2006; Whiffin et al. 2007):

$$CO(NH_2)_2 + 2H_2O \rightarrow 2NH_4^+ + CO_3^{2-} \quad (1)$$

$$Ca^{2+} + CO_3^{2-} \rightarrow CaCO_3(s) \quad (2)$$

[1]Professor, Key Laboratory of New Technology for Construction of Cities in Mountain Area, Chongqing Univ., Chongqing 400045, China; Researcher, State Key Laboratory of Coal Mine Disaster Dynamics and Control, Chongqing Univ., Chongqing 400030, China; Professor, School of Civil Engineering, Chongqing Univ., Chongqing 400045, China (corresponding author). ORCID: https://orcid.org/0000-0002-9411-4660. Email: hhuxyanson@163.com; xiaoyanganson@aliyun.com

[2]Professor, School of Civil and Construction Engineering, Oregon State Univ., Corvallis, OR 97331. ORCID: https://orcid.org/0000-0002-6265-9906. Email: Armin.Stuedlein@oregonstate.edu

[3]Graduate Student, School of Civil Engineering, Chongqing Univ., Chongqing 400045, China. Email: zhengyupanmicp@cqu.edu.cn

[4]Professor and Vice President, School of Civil Engineering, Chongqing Univ., Chongqing 400450, China. Email: cehliu@cqu.edu.cn

[5]Professor, School of Civil and Construction Engineering, Oregon State Univ., Corvallis, OR 97331. ORCID: https://orcid.org/0000-0002-8457-7602. Email: matt.evans@oregonstate.edu

[6]Ph.D. Candidate, School of Civil Engineering, Chongqing Univ., Chongqing 400045, China. Email: medihe@163.com

[7]Assistant Professor, Dept. of Civil and Environmental Engineering, Louisiana State Univ., Baton Rouge, LA 70803. ORCID: https://orcid.org/0000-0002-1641-4588. Email: thomashailin@outlook.com

[8]Professor, School of Civil and Environmental Engineering, Nanyang Technological Univ., 10 Blk N1, 50 Nanyang Ave., Singapore 639798. ORCID: https://orcid.org/0000-0003-1404-1834. Email: cjchu@ntu.edu.sg

[9]Associate Professor, Center for Bio-mediated and Bio-inspired Geotechnics, Arizona State Univ., Tempe, AZ 85287-3005. ORCID: https://orcid.org/0000-0002-5050-0260. Email: leon.vanpaassen@asu.edu

Note. This manuscript was submitted on December 14, 2019; approved on July 14, 2020; published online on October 8, 2020. Discussion period open until March 8, 2021; separate discussions must be submitted for individual papers. This technical note is part of the ***Journal of Geotechnical and Geoenvironmental Engineering***, © ASCE, ISSN 1090-0241.

Stuedlein (2008) evaluated the performance of partially-cemented and fully-cemented stone columns as a ground improvement alternative, and pointed out that this approach was particularly effective for stone columns that must bridge through locally soft and weak soils. However, this approach considered cementitious materials. Lin et al. (2016) presented a concept of a biogrouted-type ground improvement that enhanced the shaft resistance by cementing the surrounding sand. This biogrout significantly increased the shaft resistance of permeable piles under axial compression (Lin et al. 2016) and pullout loading (Lin et al. 2018). However, the effect of biogrouting on toe-bearing resistance was not effectively realized because of the long travel path for the flow of bacteria, urea, and cementation media to the pile toe, resulting in calcium carbonate ($CaCO_3$) clogs along the flow path.

This technical paper aims to evaluate the feasibility of applying the biogrouting method to precast concrete piles at the pile toe. To validate the feasibility of this method, the load-bearing performance of biogrout-improved and unimproved precast concrete piles was evaluated using model-scale experiments. The cemented soil strength and the effective zone of cementation were measured to assess the effectiveness of biogrout to improve the mechanical properties of the sand below the pile toe. The results show that the capacity of the biogrouted pile toe increased significantly because of the volumetric extent of cementation developed as result of the biogrout treatment.

Materials Used in Biogrouting

Calcareous Sand

The calcareous sand used in this study and shown in Fig. 1(a) was primarily composed of shell fragments and coral fragments (Xiao et al. 2019c) and was collected from an island in the South China Sea. The percent passing by weight and percent retained by weight of this sand are shown in Figs. 1(a and b), respectively. The mean particle size, coefficient of uniformity, and coefficient of curvature are 0.49 mm, 3.06, and 1.11, respectively. Based on the Unified Soil Classification System (ASTM 2017), the test sand is classified as poorly-graded (SP). The particle shape of this sand is predominantly subangular to subrounded, as shown in the scanning electron microscope (SEM) image from Fig. 1(c). The coral fragments are characterized by numerous internal pores as clearly shown in Fig. 1(d). The specific gravity of this sand is 2.79, while its minimum and maximum void ratios are 0.942 and 1.428 according to standards (ASTM 2016a, b).

A series of isotropically-consolidated undrained triaxial (ICU) tests were conducted on the calcareous sand at confining pressures ranging from 25 to 100 kPa to obtain the shear strength of the material. Cylindrical specimens of 38 mm in diameter and 76 mm in length were prepared using the under-compaction method (Ladd 1978) to achieve a relative density (I_D) of 0.51 (equal to that of the sand sample for a model pile, described subsequently). The dry calcareous sand mixed with 6% deaired water by weight was divided into six equal parts as six layers. Each layer that was placed into a split mold was prepared with its relative density slightly greater (1%) than the relative density of the layer below it (Belkhatir et al. 2011). This method can compensate for the increase in density of the lower layers because of the compaction effort transmitted from overlying layers to obtain a homogeneous specimen of uniform density over the specimen height, as pointed out by Polito and Martin (2001). The tests were carried out at a displacement rate of 0.2 mm/min until approximately 30% axial strain (Fig. 2). Based on the results of the ICU test series, the calcareous sand exhibited a failure stress ratio of approximately 1.47 ($M = q/p'$ where q and p' are the deviatoric stress and mean effective stress, respectively), yielding the critical-state friction angle of 36.2° {$\phi' = \text{asin}[3M/(6+M)]$}.

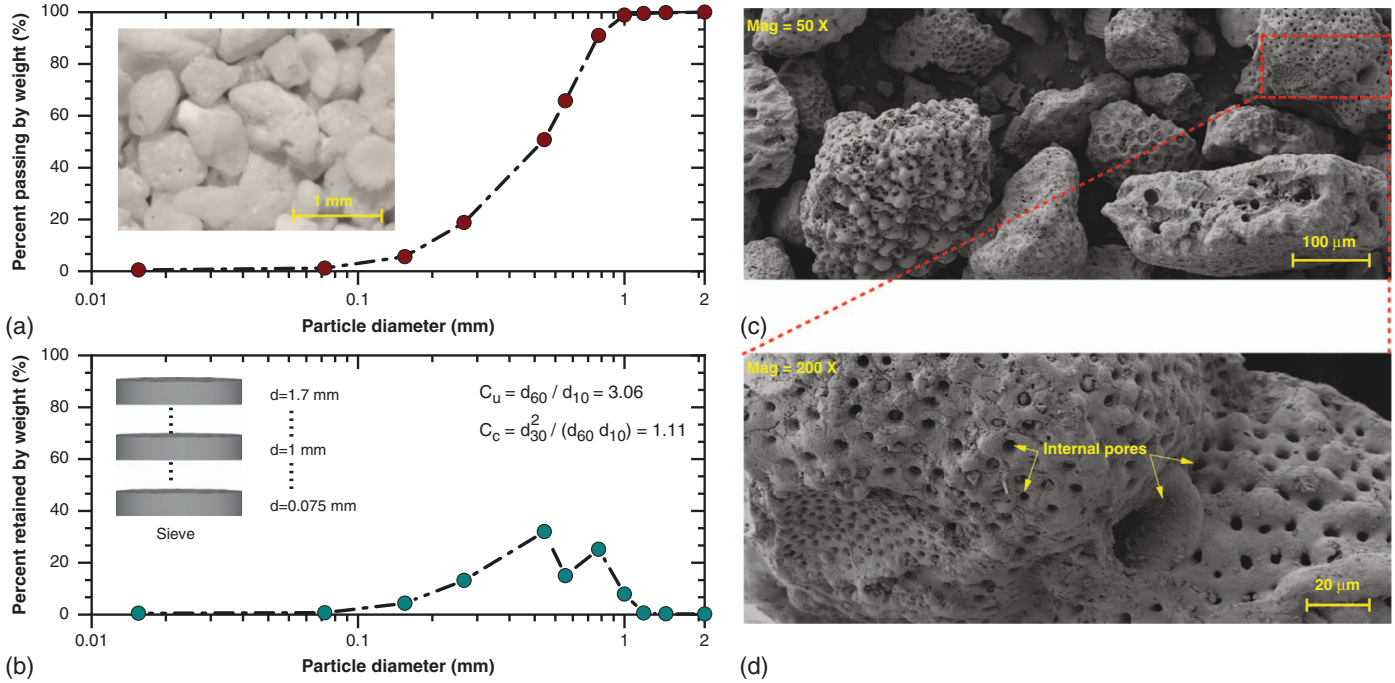

Fig. 1. (Color) Characterization of the calcareous sand used in this study: (a) particle size distribution; (b) particle size density curve; (c) SEM image of the calcareous sand with the magnification of 50; and (d) SEM image of the calcareous sand with the magnification of 200.

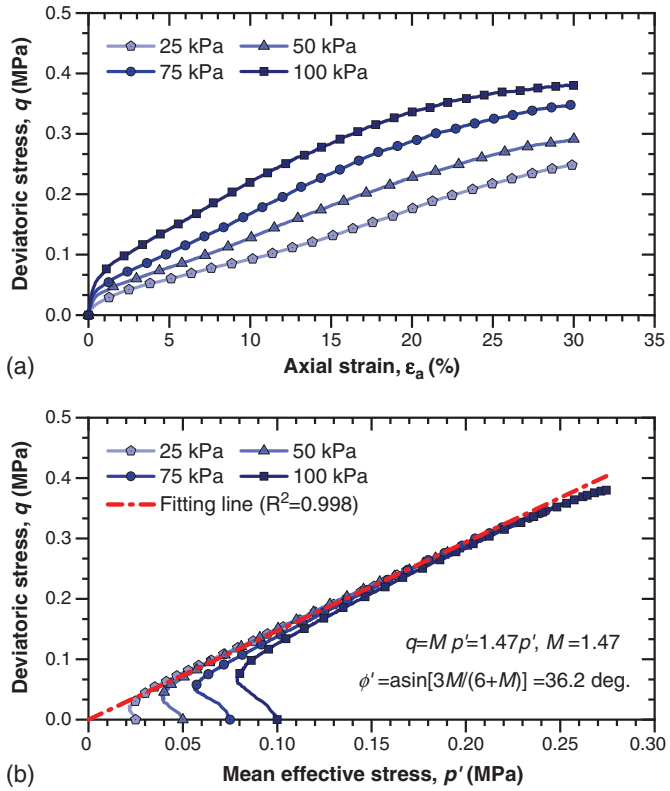

Fig. 2. (Color) Shear behavior of the tested calcareous sand: (a) deviator stress versus axial strain; and (b) effective stress path and failure line.

Bacteria and Cementation Solution

Alkaliphilic bacteria of *Sporosarcina pasteurii* [American Type Culture Collection (ATCC) 11859] was used to produce the biogrout. The medium used for the bacterial cultivation consisted of 20 g/L yeast extract, 10 g/L NH_4Cl, 12 mg/L $MnCl_2 \cdot H_2O$, and 24 mg/L $NiCl_2 \cdot 6H_2O$ with pH adjusted to 9.0 using NaOH (Xiao et al. 2020). The bacteria were cultivated in an incubator shaker at 200 revolutions per minute and 30°C for 36 h to reach an optical density of 0.8–1.0. The bacteria were centrifuged at 4,000 *g* for 20 min and then resuspended by 0.9% sodium chloride solution. The urease activity of the bacterial solution was found to be approximately 1.8 mM urea/min using the method proposed by Whiffin (2004). The bacteria were stored in a refrigerator at 4°C until application (Mortensen et al. 2011). The cementation solution used in the biogrouting process consisted of 0.5 mol/L $CaCl_2$ and 0.5 mol/L urea (Cheng et al. 2013).

Experimental Details and Test Procedures

Test Pile and Pile Installation

Two test series were conducted: *Test Series I*, representing the biogrouted model concrete pile, and *Test Series II*, focusing on the unimproved model concrete pile. A test chamber, shown in Fig. 3(a), consisting of an acrylic cuboid box reinforced by an aluminum beam and a reaction frame, was used to evaluate the performance of the model concrete piles. The dimensions of the chamber are 600 mm in width and 1,000 mm in height. The precast concrete model pile was 50 mm in diameter and 640 mm in length, as shown in Fig. 3(a). In order to accommodate delivery of biogrout

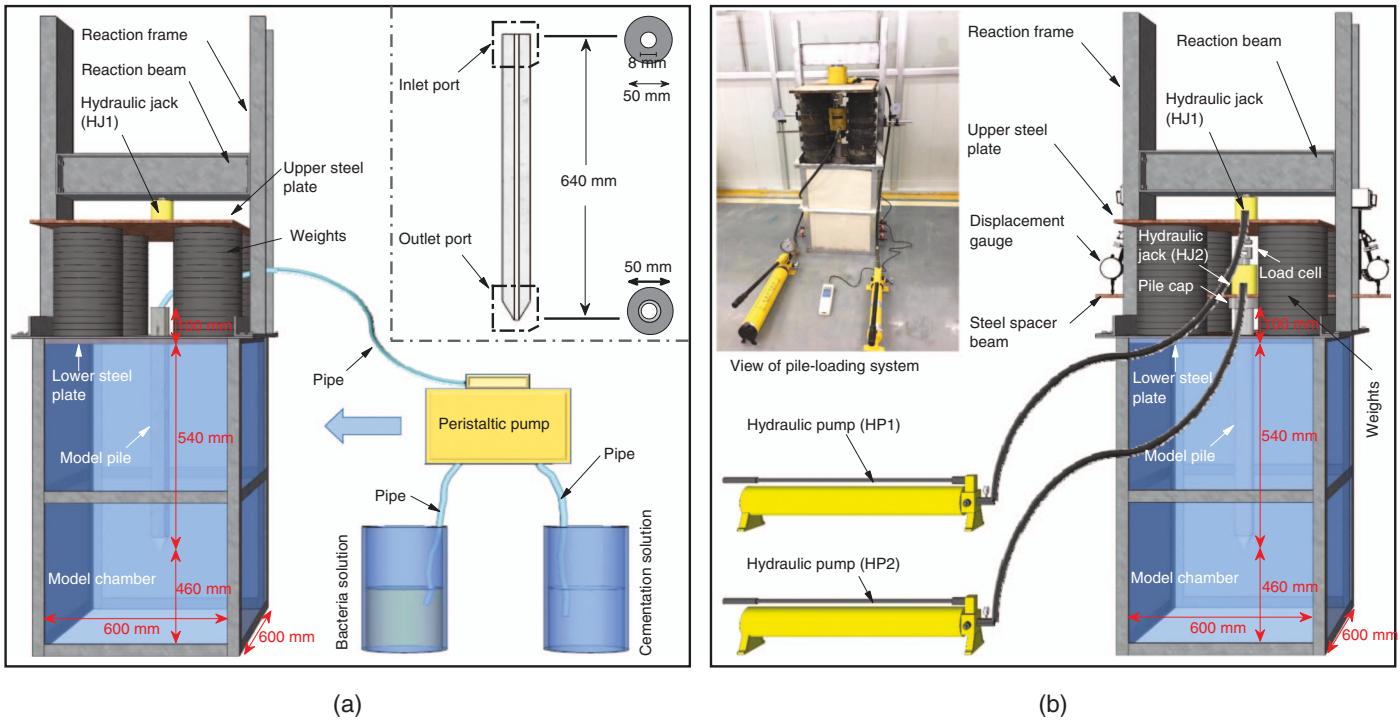

Fig. 3. (Color) Model chamber and loading system: (a) schematic diagram of the model chamber with biogrouting system and test pile; and (b) schematic diagram and photograph of the test pile loading system.

J. Geotech. Geoenviron. Eng., 2020, 146(12): 06020026

to the pile toe, a silicone tube with an inner diameter of 8 mm, and inlet and outlet ports at the pile head and toe, were positioned along the pile axis prior to casting the model concrete pile. The sand sample was prepared in layers and had 50 layers in total. Each layer that was placed into the chamber was prepared with its relative density slightly greater (1%) than that of the lower layer using the undercompaction method (Ladd 1978; Polito and Martin 2001; Belkhatir et al. 2011). The final relative density of the sand sample, i.e., 0.51, was determined by the total mass and target volume of the sand in the chamber. When the depth of the sand sample reached 460 mm in thickness, the model pile was placed on top of the sand sample to just bear on it and was supported using a supporting frame. An additional 540 mm thickness of sand was pluviated and compacted around the pile using the procedure described earlier to result in an embedded pile length of 540 mm.

In order to evaluate the response of the model concrete pile at stress magnitudes more representative of the field conditions, the stress state was raised using a surcharging system. A lower steel plate with thickness equal to 18 mm and with a circular hole in the center to allow free passage of the pile was placed on the surface of the sand sample to allow placement of a uniformly distributed stack of 5 kg weights. An upper steel plate of 18 mm thickness was placed on the stack of weights to facilitate placement of a hydraulic jack (HJ1) between the plate and the reaction frame. HJ1 was used to apply a total surcharge pressure of 50 kPa at the surface of the sand sample.

Delivery of Biogrout to the Pile Toe

The silicone tube cast within the model pile facilitated delivery of the bacteria and cementation solution. A two-phase injection strategy (Martinez et al. 2013; Safavizadeh et al. 2019) was used in this study, and consisted of the injection of bacterial solution followed by injection of cementation solution. The criteria for selecting the injection rate are as follows: (1) to maintain the production efficiency of $CaCO_3$ (Al Qabany et al. 2012); (2) to avoid the erosion of $CaCO_3$ crystals and small-sized grains (Jiang et al. 2017); and (3) to prevent the clogging of the sand because of $CaCO_3$ precipitation close to the injection well (Safavizadeh et al. 2019). The injection rate cannot be too fast based on the former two criteria and cannot be too slow based on the last criterion. An injection rate of 100 mL/h meets these criteria and was used in this study for the improvement of sand below the model pile.

For *Test Series I*, the process in the first phase initiated with pumping 200 mL of bacteria solution at the rate of 100 mL/h, as shown in Fig. 3(a). The bacteria solution was allowed to percolate through the sand sample from the pile toe. A retention of 2 h after the injection of bacteria solution was adopted to allow bacteria to attach to sand particles. In the second phase, 1,000 mL of cementation solution was pumped into the sand sample at the same rate. The sand sample was then cured for 10 h to allow the minerals to precipitate and bond the sand particles. The two-phase injection procedure lasted 24 h, which was repeated six times. Increasing urease activity is the most effective way to expedite the procedure (Hammad et al. 2013), which needs to be further studied. For comparison, the bacteria solution used in *Test Series I* was replaced with deionized water for the untreated pile in *Test Series II* with all other test conditions remaining the same.

Loading System

Axial loading tests were carried out to evaluate the improvement in toe-bearing capacity of the model concrete piles. In order to deliver the necessary pile displacement, a steel loading cap was placed on the pile head, and the hydraulic jack (HJ2) and a load cell were placed on the cap in series and shimmed with a steel spacer beam to engage the upper steel plate [Fig. 3(b)]. Two displacement dial gauges mounted to the steel test chamber and placed on the steel spacer beam resting on the pile head were used to measure the vertical displacement. The axial load was applied in increments of 0.2 kN using HJ2 and was kept constant until the penetration rate was less than 0.01 mm/min (Yasufuku and Hyde 1995; ASTM 2013). The application of load was terminated when the pile head displacement continued with little or no increase in bearing resistance.

Evaluation of the Biogrout Strength

The uncemented sand above the toe of the model concrete pile was gently removed without disturbing the cemented sand after the axial loading test of *Test Series I*. The biocemented sand was found below the pile-toe elevation. A pocket penetrometer was used to investigate the strength and distribution of the biocemented sand (Cheng and Cord-Ruwisch 2012). The pocket penetrometer test was performed by pushing the penetrometer tip on the biocemented sand at a target location, and the unit tip resistance corresponding to the fracture of the biocemented sand was recorded as the penetration strength at that location. $CaCO_3$ formed heterogeneously below the model pile toe during the MICP-treating process, and the strength of the biocemented sand varied vastly as a function of the location with respect to the pile toe. Since a penetrometer tip has a specific range in calibrated strength, several tips with different strength ranges were used depending on the strength of the biocemented sand to ensure the accuracy of the measurements. Each tip with the strength gage was calibrated to ensure consistent readings prior to measuring penetration strength. Measurements were made at different locations with respect to the pile toe. At least four measurements were conducted at each selected location.

Experimental Results and Discussion

Load-Displacement Pile Response

Fig. 4(a) shows the axial stress applied to the pile head, q_{pile}, versus the displacement, δ, normalized by the pile head diameter, D, for the untreated pile with the confining pressure of 50 kPa at the surface of the sand sample. The axial stress q_{pile} is defined as $q_{pile} = Q_{\text{total}}/(\pi D^2/4)$ where Q_{total} is the total resistance. For the purposes of comparison to previous studies on pile load tests, the ultimate bearing resistance of the pile was interpreted from the q_{pile}-δ/D curves at $\delta/D = 0.1$ (Briaud and Tucker 1988; Neely 1991; Lee and Salgado 1999; Briaud et al. 2000; Comodromos et al. 2003; Paik and Salgado 2003; Paik et al. 2003; Randolph 2003; Gavin and Lehane 2007; Xu et al. 2008; Seo et al. 2009; Basu and Salgado 2014; Han et al. 2017a, b, 2019a, b). The bearing capacity of the pile in the calcareous sand with $I_D = 0.51$ for *Test Series II* was 1.16 MPa in this work. This was higher than 0.76 MPa of the pile in the calcareous sand with $I_D = 0.4$ but lower than 1.91 MPa of the pile in the calcareous sand with $I_D = 0.9$ under a surcharge of 50 kPa from the work by Yasufuku and Hyde (1995) where the pile diameter and embedded pile length was 20 and 90 mm, respectively. This basic trend of the bearing capacity with relative density is reasonable as anticipated in previous studies (Meyerhof 1977; Kuwajima et al. 2009; Reddy and Stuedlein 2017), although the differences in the gradation of calcareous sand could also affect the bearing capacity.

Fig. 4(b) presents the q_{pile}-δ/D response of the biogrouted pile tested in this study in comparison to the biogrouted pervious concrete pile reported by Lin et al. (2016). The total resistance

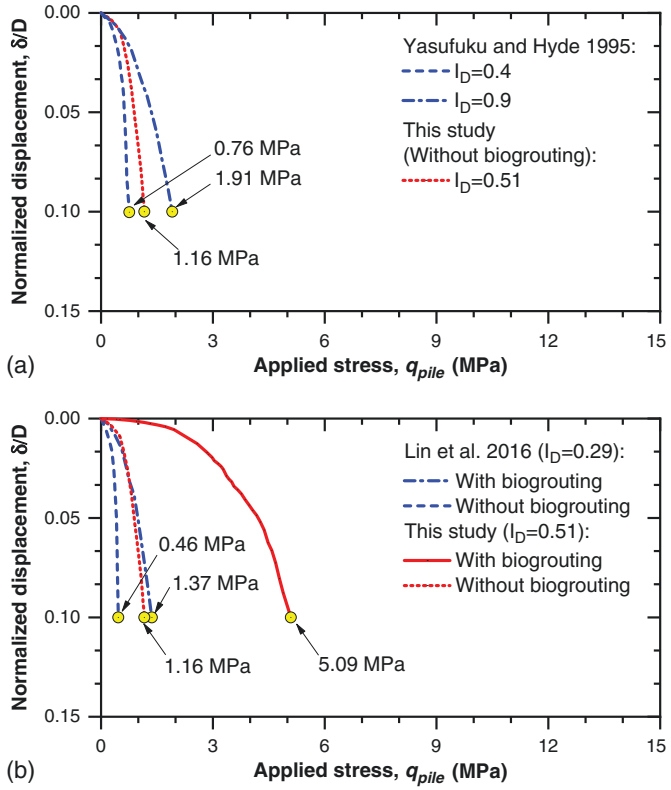

Fig. 4. (Color) Normalized settlement against applied pile stress: (a) comparison of the untreated pile in this study to the results reported by Yasufuku and Hyde (1995); and (b) comparison of biogrouted pile in this study and Lin et al. (2016).

observed for the biogrouted pile bearing in calcareous sand with $I_D = 0.51$ was 5.09 MPa, which was approximately 4.4 times as large as that of the untreated pile in this study. In the study (Lin et al. 2016), the total resistance for biogrouted pervious concrete pile bearing in poorly graded sand with $I_D = 0.29$ was approximately three times as large as that of the untreated pervious concrete pile. Biogrout around the shaft of the pervious concrete pile in Lin et al. (2016, 2018) mainly increased the shaft resistance, whereas the biogrout at the pile toe in this study mainly enhances the toe bearing resistance, as revealed in the forensic investigation described subsequently.

In order to estimate the increase in toe bearing resistance resulting from the biogrout treatment, a simplified load transfer analysis was conducted. The average unit shaft resistance, f_s, associated with piles in normally-consolidated granular soils is commonly computed using the following equation (Neely 1991; Stuedlein et al. 2012; Reddy and Stuedlein 2017):

$$f_s = \sigma'_{v0} K_s \tan\delta' = \sigma'_{v0} K_s \tan\phi' \tag{3}$$

where σ'_{v0} = average vertical effective stress; K_s = horizontal earth pressure coefficient; and δ' = interface friction angle. In the current study, δ' is assumed equal to ϕ', as the normalized interface roughness of the model pile is close to the threshold value of about 0.3 (Han et al. 2018; Rauthause et al. 2020).

By experimental design, the magnitude of the shaft resistance for the biogrouted pile is the same as that of the untreated pile. The shaft resistance, Q_s, is calculated as

$$Q_s = f_s A_s \tag{4}$$

where A_s = area of the shaft. The toe-bearing resistance of the model piles of *Test Series I* and *Test Series II* was calculated using the following equations:

$$Q_t = Q_{total} - Q_s \tag{5}$$

where Q_t = toe-bearing resistance, respectively.

According to Eqs. (3)–(5), biogrouting at the pile toe in this study greatly increased the toe shearing resistance from 0.92 kN (i.e., $Q_t = Q_{total} - Q_s = 2.28–1.36 = 0.92$ kN) for the untreated model pile to 8.63 kN (i.e., $Q_t = Q_{total} - Q_s = 9.99–1.36 = 8.63$ kN) for the biogrouted model pile while the shaft resistance of the biogrouted model pile was not changed as the sand around the shaft was not improved. Thus, the toe-bearing resistance of the biogrouted model pile was 9.4 (= 8.63/0.92) times as large as that of the untreated model pile.

Distribution of Measured Point Strength Below the Pile Toe

Penetration strength tests were performed at different locations below the pile toe as the biocemented sand below the pile toe was excavated layer by layer. Based on these test data, the spatial distribution of the strength of the biocemented sand was reconstructed using MATLAB version R2018a in a Cartesian coordinate system with the origin fixed at the pile toe, as shown in Fig. 5. Figs. 5(a and b) show the strength distribution at cross sections with $x = 0$ cm and $y = 0$ cm, respectively. Figs. 5(a and b) clearly show that the strength was highest near the pile toe and decreased with increasing distance from the pile toe. Biocemented sand specimens at four locations were carefully collected to investigate effect of depth and radius on the strength and microstructures using SEM images (as will be introduced in the next section). Position A ($x = 0$ cm, $y = 0$ cm, $z = 0$ cm) and Position B ($x = 0$ cm, $y = 0$ cm, $z = 10$ cm) are shown in Fig. 5(a) to indicate the depth-dependent distribution of strength. The strength below the pile toe decreased from 710 kPa (at Position A) to 330 kPa (at Position B), as depth increased from 0 to 10 cm. Fig. 5(b) shows that the strength decreased from 290 kPa at position C ($x = 2.8$ cm, $y = 0$ cm, $z = 15$ cm) to 21 kPa at Position D ($x = 13.5$ cm, $y = 0$ cm, $z = 15$ cm), as the radius increased.

Moreover, as presented in Figs. 5(a and b), variation in strength was observed at different locations with the same depth and radius but in different directions (i.e., strength distribution was asymmetric), which is attributed to the heterogeneity during the biogrouting process (DeJong et al. 2006; Ivanov and Chu 2008; van Paassen et al. 2010b; Lin et al. 2016; Jiang and Soga 2017; Lin et al. 2018; Nassar et al. 2018; Gomez et al. 2019; Pan et al. 2019; Wang et al. 2019). The previously mentioned phenomena suggest that when the bacteria and cementation fluid flowed from the outlet port, calcium carbonate was generated along the preferential flow path that was influenced by gravity and local $CaCO_3$ clogging, as also reported by van Paassen et al. (2010b). The calcium carbonate cementation gradually decreased along the seepage path and away from the pile toe because of a decrease in urease activity with increasing distance from the outlet port, as pointed out by Whiffin et al. (2007) and Nassar et al. (2018). On the other hand, the heterogeneous distribution of the calcium carbonate also affected the distribution of strength.

Fig. 5(c) presents a reconstructed biogrout bulb with spatially-varying strength computed by removing those locations with zero

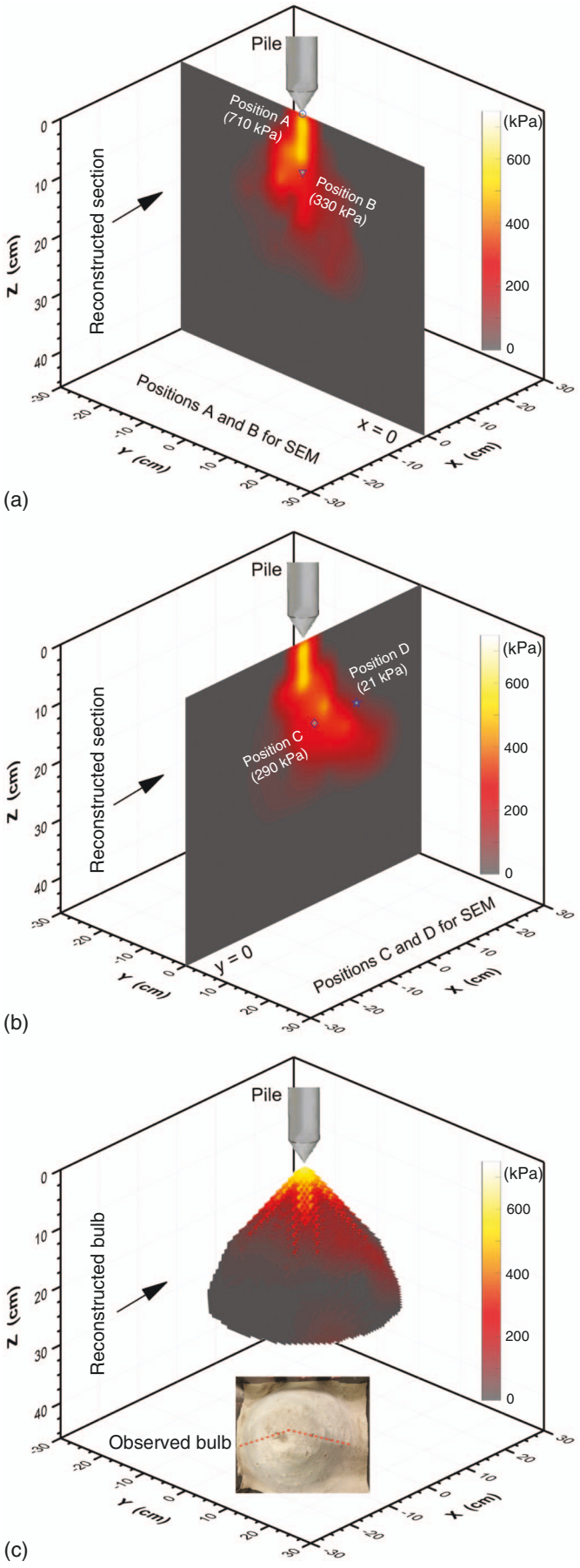

Fig. 5. (Color) Strength distribution of biocemented sand below the pile toe: (a) $x = 0$ cm; (b) $y = 0$ cm; and (c) biocemented sand bulb.

strength from all sections including two sections in Figs. 5(a and b), which is similar to the observed biogrout bulb. Note that the strength measured after the pile loading test is lower than the initial pretest strength, such that these measurements are biased to a degree following the penetration-imposed shear and axial strains within the biogrouted sand. Thus, the measured strength represents the cementation strength that remained following loading.

Microstructure of Cemented Calcareous Sand

Considering the changes in the strength shown in Fig. 5, a strong correlation between the presence of calcium carbonate and the cemented sand strength was speculated, where the higher the calcium content, the higher the strength measured. Fig. 6 shows the microstructure of the biocemented calcareous sand at four positions in Figs. 5(a and b). Figs. 6(a and b) show the microscale properties of the biocemented sands at Position A and Position B from different depths shown in Fig. 5(a). A greater amount of large crystals was observed in Fig. 6(a) than that observed in Fig. 6(b), which leads to a higher strength of the biocemented sand at Position A than that at Position B, as shown in Fig. 5(a). Figs. 6(c and d) show the microscale properties of the biocemented sands at Position C and Position D (the same depth) with different radii shown in Fig. 5(b). A tendency of decreasing calcium carbonate with increasing radius was observed in Figs. 6(c and d), leading to a decrease in the average strength with increasing radius, as mentioned before in Fig. 5(b). In summary, the amount of calcium carbonate decreased radially and vertically with increasing distance from the pile toe.

Based on the amount, distribution, and morphology of $CaCO_3$, four stages for $CaCO_3$ precipitation could be distinguished, namely, particle-pore patching, particle coating, particle bonding, and void filling. During the first stage, calcium carbonate precipitated at the particle surfaces, which led to particle-pore patching of the coral sand structure, as shown in Fig. 6(d). During second stage, as the amount of calcium carbonate increased, the sand particles became coated and gradually enveloped by crystals, as depicted in Figs. 6(a–d). During third stage, bonds may have formed at the point of contact of the sand particles, as depicted in Figs. 6(a–c). During the fourth stage, as the precipitation of calcium carbonate further increases, large crystals grow epitaxially and fill the void of the sand matrix, as shown in Fig. 6(a). These stages for $CaCO_3$ precipitation in calcareous sand would be different from that in silica sand where relatively large crystals were observed in MICP treatment. The differences in the precipitation pattern can be attributed to the differences in precipitation mechanisms. The $CaCO_3$ crystals in calcareous sand can grow immediately on the existing grain surfaces, because the mineral of calcareous sand is $CaCO_3$ and grain surface of calcareous sand can be interpreted as crystal nucleation. Thus, the $CaCO_3$ crystals could be precipitated as sheets of tiny calcite crystals to patch internal pores of calcareous sand or coat grain surfaces of calcareous sand, as observed in Figs. 6(c–d). In contrast, the $CaCO_3$ precipitation in silica sands involves crystal nucleation for growth of relatively large crystals (Kim et al. 2020).

Conclusions

This technical paper presents research on a novel biogrouted precast concrete pile. The toe-bearing capacities of piles with and without biogrouting in calcareous sand was compared using model tests. The strength of the biocemented sand below the biogrouted pile toe was measured with a pocket penetrometer. Additionally, SEM images of cemented sand samples were also presented. The following conclusions can be drawn from this study:

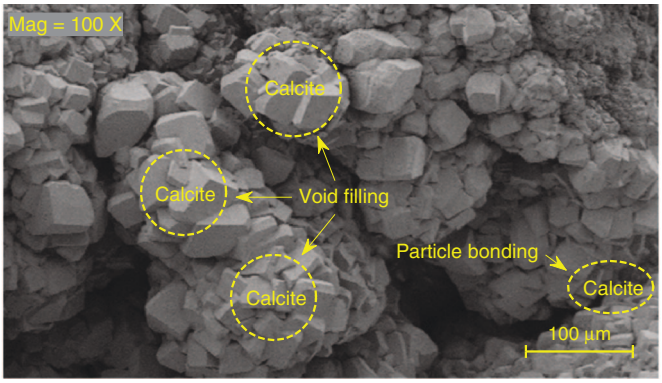

(a)

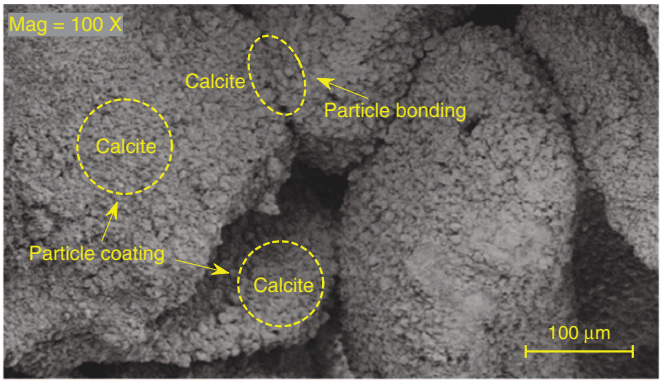

(b)

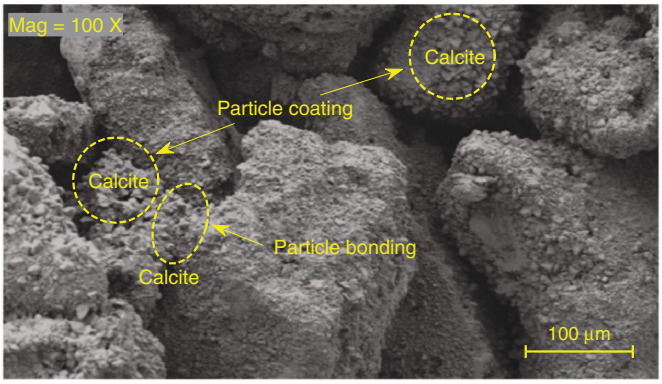

(c)

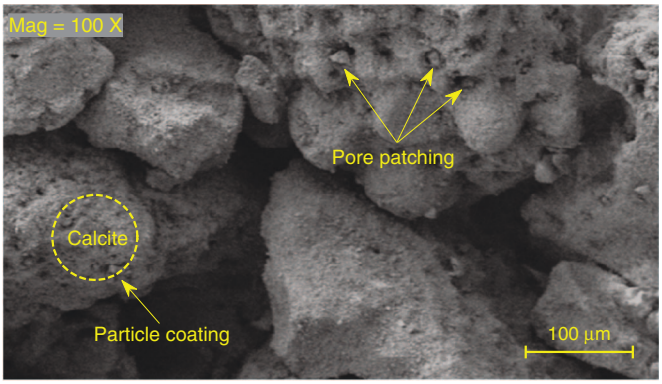

(d)

Fig. 6. (Color) SEM images of biocemented sand below the pile toe: (a) Position A; (b) Position B; (c) Position C; and (d) Position D.

1. The total resistance of the biogrouted pile in calcareous sand with the relative density of 0.51 was approximately 4.4 times as large as that of the untreated pile bearing in the same sand with the same relative density. The enhanced capacity of the precast biogrouted pile was attributed to the increase in toe-bearing resistance which was about 9.4 times as large as that of the untreated pile.
2. The average strength of the biocemented sand below the biogrouted pile toe gradually decreased as the vertical distance or lateral distance from the pile toe increased according to the test results for estimating the spatial distribution of strength using a penetrometer. The strength distribution was also verified by the distribution of calcium carbonate obtained from SEM images where the amount of calcium carbonate decreased radially and vertically from the pile toe. The calcium carbonate exhibited four effects: particle-pore patching, particle coating, particle bonding, and void filling. Increasing the amount of calcium carbonate led to an increase in particle bonding.

Data Availability Statement

Some or all data, models, or code generated or used during the study are available from the corresponding author by request.

Acknowledgments

The authors would like to acknowledge the financial support from the National Science Foundation of China (Grant Nos. 41831282, 51922024, 51678094, and 51578096). TME was supported by the U.S. National Science Foundation (Grant No. CMMI-1933355) during this work. This support is gratefully acknowledged.

Notation

The following symbols are used in this paper:

A_s = area of the pile shaft (mm^2);
D = pile head diameter (mm);
f_s = average unit shaft resistance (MPa);
I_D = relative density;
K_s = horizontal earth pressure coefficient;
$\bar{l}$ = average lateral distance (cm);
M = failure stress ratio;
p' = mean effective stress (MPa);
Q_s = shaft resistance (kN);
Q_t = toe bearing resistance (kN);
Q_{total} = total resistance (kN);
q = deviatoric stress (MPa);
q_{pile} = axial stress applied to the pile head (MPa);
x, y, z = spatial position in the Cartesian coordinate (cm);
δ = displacement of the pile head (mm);
δ' = interface friction angle (degree);
σ'_{v0} = average vertical effective stress (MPa); and
ϕ' = failure friction angle (degree).

References

Al Qabany, A., and K. Soga. 2013. "Effect of chemical treatment used in MICP on engineering properties of cemented soils." *Géotechnique* 63 (4): 331–339. https://doi.org/10.1680/geot.SIP13.P.022.

Al Qabany, A., K. Soga, and C. Santamarina. 2012. "Factors affecting efficiency of microbially induced calcite precipitation." *J. Geotech.*

Geoenviron. Eng. 138 (8): 992–1001. https://doi.org/10.1061/(ASCE)GT.1943-5606.0000666.

ASTM. 2013. *Standard test methods for deep foundations under static axial compressive load*. ASTM D1143/D1143M-07. West Conshohocken, PA: ASTM.

ASTM. 2016a. *Standard test method for maximum index density and unit weight of soils using vibratory table*. ASTM D4253-16. West Conshohocken, PA: ASTM.

ASTM. 2016b. *Standard test methods for minimum index density and unit weight of soils and calculation of relative density.* ASTM D4254-16. West Conshohocken, PA: ASTM.

ASTM. 2017. *Standard practice for classification of soils for engineering purposes (unified soil classification system)*. ASTM D2487-17. West Conshohocken, PA: ASTM.

Bandini, V., and M. R. Coop. 2011. "The influence of particle breakage on the location of the critical state line of sands." *Soils Found.* 51 (4): 591–600. https://doi.org/10.3208/sandf.51.591.

Basu, D., and R. Salgado. 2014. "Closure to 'load and resistance factor design of drilled shafts in sand' by D. Basu and Rodrigo Salgado." *J. Geotech. Geoenviron. Eng.* 140 (3): 07014002. https://doi.org/10.1061/(ASCE)GT.1943-5606.0001055.

Belkhatir, M., A. Arab, T. Schanz, H. Missoum, and N. Della. 2011. "Laboratory study on the liquefaction resistance of sand-silt mixtures: Effect of grading characteristics." *Granular Matter* 13 (5): 599–609. https://doi.org/10.1007/s10035-011-0269-0.

Briaud, J. L., M. Ballouz, and G. Nasr. 2000. "Static capacity prediction by dynamic methods for three bored piles." *J. Geotech. Geoenviron. Eng.* 126 (7): 640–649. https://doi.org/10.1061/(ASCE)1090-0241(2000)126:7(640).

Briaud, J. L., and L. M. Tucker. 1988. "Measured and predicted axial response of 98 piles." *J. Geotech. Eng.* 114 (9): 984–1001. https://doi.org/10.1061/(ASCE)0733-9410(1988)114:9(984).

Burbank, M., T. Weaver, R. Lewis, T. Williams, B. Williams, and R. Crawford. 2013. "Geotechnical tests of sands following bioinduced calcite precipitation catalyzed by indigenous bacteria." *J. Geotech. Geoenviron. Eng.* 139 (6): 928–936. https://doi.org/10.1061/(ASCE)GT.1943-5606.0000781.

Cheng, L., and R. Cord-Ruwisch. 2012. "In situ soil cementation with ureolytic bacteria by surface percolation." *Ecol. Eng.* 42 (May): 64–72. https://doi.org/10.1016/j.ecoleng.2012.01.013.

Cheng, L., R. Cord-Ruwisch, and M. A. Shahin. 2013. "Cementation of sand soil by microbially induced calcite precipitation at various degrees of saturation." *Can. Geotech. J.* 50 (1): 81–90. https://doi.org/10.1139/cgj-2012-0023.

Cheng, L., and M. A. Shahin. 2016. "Urease active bioslurry: A novel soil improvement approach based on microbially induced carbonate precipitation." *Can. Geotech. J.* 53 (9): 1376–1385. https://doi.org/10.1139/cgj-2015-0635.

Cheng, L., and M. A. Shahin. 2017. "Stabilisation of oil-contaminated soils using microbially induced calcite crystals by bacterial flocs." *Geotech. Lett.* 7 (2): 146–151. https://doi.org/10.1680/jgele.16.00178.

Cheng, L., M. A. Shahin, and D. Mujah. 2017. "Influence of key environmental conditions on microbially induced cementation for soil stabilization." *J. Geotech. Geoenviron. Eng.* 143 (1): 04016083. https://doi.org/10.1061/(ASCE)GT.1943-5606.0001586.

Chou, C.-W., E. A. Seagren, A. H. Aydilek, and M. Lai. 2011. "Biocalcification of sand through ureolysis." *J. Geotech. Geoenviron. Eng.* 137 (12): 1179–1189. https://doi.org/10.1061/(ASCE)GT.1943-5606.0000532.

Chu, J., V. Ivanov, M. Naeimi, V. Stabnikov, and B. Li. 2013. "Microbial method for construction of an aquaculture pond in sand." *Géotechnique* 63 (10): 871–875. https://doi.org/10.1680/geot.SIP13.P.007.

Comodromos, E. M., C. T. Anagnostopoulos, and M. K. Georgiadis. 2003. "Numerical assessment of axial pile group response based on load test." *Comput. Geotech.* 30 (6): 505–515. https://doi.org/10.1016/S0266-352X(03)00017-X.

Coop, M. R. 1990. "The mechanics of uncemented carbonate sands." *Géotechnique* 40 (4): 607–626. https://doi.org/10.1680/geot.1990.40.4.607.

Coop, M. R., K. K. Sorensen, T. Bodas Freitas, and G. Georgoutsos. 2004. "Particle breakage during shearing of a carbonate sand." *Géotechnique* 54 (3): 157–163. https://doi.org/10.1680/geot.2004.54.3.157.

Cui, M., J. Zheng, R. Zhang, H. Lai, and J. Zhang. 2017. "Influence of cementation level on the strength behaviour of bio-cemented sand." *Acta Geotech.* 12 (5): 971–986. https://doi.org/10.1007/s11440-017-0574-9.

DeJong, J. T., M. B. Fritzges, and K. Nüsslein. 2006. "Microbially induced cementation to control sand response to undrained shear." *J. Geotech. Geoenviron. Eng.* 132 (11): 1381–1392. https://doi.org/10.1061/(ASCE)1090-0241(2006)132:11(1381).

DeJong, J. T., B. M. Mortensen, B. C. Martinez, and D. C. Nelson. 2010. "Bio-mediated soil improvement." *Ecol. Eng.* 36 (2): 197–210. https://doi.org/10.1016/j.ecoleng.2008.12.029.

Doherty, P., G. Spagnoli, and D. Bellato. 2016. "Mixed-in-place response of two carbonate sands." *Proc. Inst. Civ. Eng. Geotech. Eng.* 169 (2): 153–163. https://doi.org/10.1680/jgeen.15.00058.

Dyson, G. J., and M. F. Randolph. 2001. "Monotonic lateral loading of piles in calcareous sand." *J. Geotech. Geoenviron. Eng.* 127 (4): 346–352. https://doi.org/10.1061/(ASCE)1090-0241(2001)127:4(346).

Gao, Y., L. Hang, J. He, and J. Chu. 2018. "Mechanical behaviour of bio-cemented sands at various treatment levels and relative densities." *Acta Geotech.* 14 (3): 697–707. https://doi.org/10.1007/s11440-018-0729-3.

Gavin, K., and B. Lehane. 2007. "Base load-displacement response of piles in sand." *Can. Geotech. J.* 44 (9): 1053–1063. https://doi.org/10.1139/T07-048.

Gomez, M. G., C. M. R. Graddy, J. T. DeJong, and D. C. Nelson. 2019. "Biogeochemical changes during bio-cementation mediated by stimulated and augmented ureolytic microorganisms." *Sci. Rep.* 9 (1): 11517. https://doi.org/10.1038/s41598-019-47973-0.

Hammad, I. A., F. N. Talkhan, and A. E. Zoheir. 2013. "Urease activity and induction of calcium carbonate precipitation by Sporosarcina pasteurii NCIMB 8841." *J. Appl. Sci. Res.* 9 (3): 1525–1533.

Han, F., E. Ganju, R. Salgado, and M. Prezzi. 2018. "Effects of interface roughness, particle geometry, and gradation on the sand–steel interface friction angle." *J. Geotech. Geoenviron. Eng.* 144 (12): 04018096. https://doi.org/10.1061/(ASCE)GT.1943-5606.0001990.

Han, F., E. Ganju, R. Salgado, and M. Prezzi. 2019a. "Comparison of the load response of closed-ended and open-ended pipe piles driven in gravelly sand." *Acta Geotech.* 14 (6): 1785–1803. https://doi.org/10.1007/s11440-019-00863-1.

Han, F., M. Prezzi, R. Salgado, and M. Zaheer. 2017a. "Axial resistance of closed-ended steel-pipe piles driven in multilayered soil." *J. Geotech. Geoenviron. Eng.* 143 (3): 04016102. https://doi.org/10.1061/(ASCE)GT.1943-5606.0001589.

Han, F., R. Salgado, M. Prezzi, and J. Lim. 2017b. "Shaft and base resistance of non-displacement piles in sand." *Comput. Geotech.* 83 (Mar): 184–197. https://doi.org/10.1016/j.compgeo.2016.11.006.

Han, F., R. Salgado, M. Prezzi, and J. Lim. 2019b. "Axial resistance of nondisplacement pile groups in sand." *J. Geotech. Geoenviron. Eng.* 145 (7): 04019027. https://doi.org/10.1061/(ASCE)GT.1943-5606.0002050.

Hyodo, M., N. Aramaki, M. Itoh, and A. F. L. Hyde. 1996. "Cyclic strength and deformation of crushable carbonate sand." *Soil Dyn. Earthquake Eng.* 15 (5): 331–336. https://doi.org/10.1016/0267-7261(96)00003-6.

Ivanov, V., and J. Chu. 2008. "Applications of microorganisms to geotechnical engineering for bioclogging and biocementation of soil in situ." *Rev. Environ. Sci. Biotechnol.* 7 (2): 139–153. https://doi.org/10.1007/s11157-007-9126-3.

Jiang, N.-J., and K. Soga. 2017. "The applicability of microbially induced calcite precipitation (MICP) for internal erosion control in gravel–sand mixtures." *Géotechnique* 67 (1): 42–55. https://doi.org/10.1680/jgeot.15.P.182.

Jiang, N.-J., K. Soga, and M. Kuo. 2017. "Microbially induced carbonate precipitation for seepage-induced internal erosion control in sand–clay mixtures." *J. Geotech. Geoenviron. Eng.* 143 (3): 04016100. https://doi.org/10.1061/(ASCE)GT.1943-5606.0001559.

Kim, D. H., N. Mahabadi, J. Jang, and L. A. van Paassen. 2020. "Assessing the kinetics and pore-scale characteristics of biological calcium carbonate precipitation in porous media using a microfluidic chip experiment."

Water Resour. Res. 56 (2): 1–19. https://doi.org/10.1029/2019WR025420.

Kuwajima, K., M. Hyodo, and A. F. L. Hyde. 2009. "Pile bearing capacity factors and soil crushability." *J. Geotech. Geoenviron. Eng.* 135 (7): 901–913. https://doi.org/10.1061/(ASCE)GT.1943-5606.0000057.

Ladd, R. S. 1978. "Preparing test specimens using undercompaction." *Geotech. Test. J.* 1 (1): 16–23. https://doi.org/10.1520/GTJ10364J.

Lade, P. V., C. D. Liggio, and J. Nam. 2009. "Strain rate, creep, and stress drop-creep experiments on crushed coral sand." *J. Geotech. Geoenviron. Eng.* 135 (7): 941–953. https://doi.org/10.1061/(ASCE)GT.1943-5606.0000067.

Lee, C. Y., and H. G. Poulos. 1988. "Effective stress dependence of pile shaft capacity in calcareous sand." *J. Geotech. Eng.* 114 (10): 1189–1193. https://doi.org/10.1061/(ASCE)0733-9410(1988)114:10(1189).

Lee, C. Y., and H. G. Poulos. 1991. "Tests on model instrumented grouted piles in offshore calcareous soil." *J. Geotech. Eng.* 117 (11): 1738–1753. https://doi.org/10.1061/(ASCE)0733-9410(1991)117:11(1738).

Lee, J. H., and R. Salgado. 1999. "Determination of pile base resistance in sands." *J. Geotech. Geoenviron. Eng.* 125 (8): 673–683. https://doi.org/10.1061/(ASCE)1090-0241(1999)125:8(673).

Lehane, B. M., J. A. Schneider, J. K. Lim, and G. Mortara. 2012. "Shaft friction from instrumented displacement piles in an uncemented calcareous sand." *J. Geotech. Geoenviron. Eng.* 138 (11): 1357–1368. https://doi.org/10.1061/(ASCE)GT.1943-5606.0000712.

Li, M., L. Li, U. Ogbonnaya, K. Wen, A. Tian, and F. Amini. 2016. "Influence of fiber addition on mechanical properties of MICP-treated sand." *J. Mater. Civ. Eng.* 28 (4): 04015166. https://doi.org/10.1061/(ASCE)MT.1943-5533.0001442.

Li, M., K. Wen, Y. Li, and L. Zhu. 2017. "Impact of oxygen availability on microbially induced calcite precipitation (MICP) treatment." *Geomicrobiol. J.* 35 (1): 15–22. https://doi.org/10.1080/01490451.2017.1303553.

Lin, H., M. T. Suleiman, H. M. Jabbour, and D. G. Brown. 2018. "Bio-grouting to enhance axial pull-out response of pervious concrete ground improvement piles." *Can. Geotech. J.* 55 (1): 119–130. https://doi.org/10.1139/cgj-2016-0438.

Lin, H., M. T. Suleiman, H. M. Jabbour, D. G. Brown, and E. Kavazanjian Jr. 2016. "Enhancing the axial compression response of pervious concrete ground improvement piles using biogrouting." *J. Geotech. Geoenviron. Eng.* 142 (10): 04016045. https://doi.org/10.1061/(ASCE)GT.1943-5606.0001515.

Mao, W., Y. Yang, W. Lin, S. Aoyama, and I. Towhata. 2018. "High frequency acoustic emissions observed during model pile penetration in sand and implications for particle breakage behavior." *Int. J. Geomech.* 18 (11): 04018143. https://doi.org/10.1061/(ASCE)GM.1943-5622.0001287.

Martinez, B. C., J. T. DeJong, T. R. Ginn, B. M. Montoya, T. H. Barkouki, C. Hunt, B. Tanyu, and D. Major. 2013. "Experimental optimization of microbial-induced carbonate precipitation for soil improvement." *J. Geotech. Geoenviron. Eng.* 139 (4): 587–598. https://doi.org/10.1061/(ASCE)GT.1943-5606.0000787.

Meyerhof, G. G. 1977. "Bearing capacity and settlement of pile foundations." *J. Geotech. Eng.* 102 (3): 197–228.

Miao, G., and D. Airey. 2013. "Breakage and ultimate states for a carbonate sand." *Géotechnique* 63 (14): 1221–1229. https://doi.org/10.1680/geot.12.P.111.

Montoya, B. M., and J. T. Dejong. 2013. "Healing of biologically induced cemented sands." *Geotech. Lett.* 3 (3): 147–151. https://doi.org/10.1680/geolett.13.00044.

Montoya, B. M., and J. T. DeJong. 2015. "Stress-strain behavior of sands cemented by microbially induced calcite precipitation." *J. Geotech. Geoenviron. Eng.* 141 (6): 04015019. https://doi.org/10.1061/(ASCE)GT.1943-5606.0001302.

Montoya, B. M., J. T. DeJong, and R. W. Boulanger. 2013. "Dynamic response of liquefiable sand improved by microbial-induced calcite precipitation." *Géotechnique* 63 (4): 302–312. https://doi.org/10.1680/geot.SIP13.P.019.

Montoya, B. M., S. Safavizadeh, and M. A. Gabr. 2019. "Enhancement of coal ash compressibility parameters using microbial-induced carbonate precipitation." *J. Geotech. Geoenviron. Eng.* 145 (5): 04019018. https://doi.org/10.1061/(ASCE)GT.1943-5606.0002036.

Mortensen, B. M., M. J. Haber, J. T. DeJong, L. F. Caslake, and D. C. Nelson. 2011. "Effects of environmental factors on microbial induced calcium carbonate precipitation." *J. Appl. Microbiol.* 111 (2): 338–349. https://doi.org/10.1111/j.1365-2672.2011.05065.x.

Murff, J. D. 1987. "Pile capacity in calcareous sands: State of the art." *J. Geotech. Eng.* 113 (5): 490–507. https://doi.org/10.1061/(ASCE)0733-9410(1987)113:5(490).

Nassar, M. K., D. Gurung, M. Bastani, T. R. Ginn, B. Shafei, M. G. Gomez, C. M. R. Graddy, D. C. Nelson, and J. T. DeJong. 2018. "Large-scale experiments in microbially induced calcite precipitation (MICP): Reactive transport model development and prediction." *Water Resour. Res.* 54 (1): 480–500. https://doi.org/10.1002/2017WR021488.

Neely, W. J. 1991. "Bearing capacity of auger-cast piles in sand." *J. Geotech. Eng.* 117 (2): 331–345. https://doi.org/10.1061/(ASCE)0733-9410(1991)117:2(331).

Nemati, M., and G. Voordouw. 2003. "Modification of porous media permeability, using calcium carbonate produced enzymatically in situ." *Enzyme Microb. Technol.* 33 (5): 635–642. https://doi.org/10.1016/S0141-0229(03)00191-1.

O'Donnell, T. S., and E. Kavazanjian Jr. 2015. "Stiffness and dilatancy improvements in uncemented sands treated through MICP." *J. Geotech. Geoenviron. Eng.* 141 (11): 02815004. https://doi.org/10.1061/(ASCE)GT.1943-5606.0001407.

Paik, K., and R. Salgado. 2003. "Determination of bearing capacity of open-ended piles in sand." *J. Geotech. Geoenviron. Eng.* 129 (1): 46–57. https://doi.org/10.1061/(ASCE)1090-0241(2003)129:1(46).

Paik, K., R. Salgado, J. Lee, and B. Kim. 2003. "Behavior of open- and closed-ended piles driven into sands." *J. Geotech. Geoenviron. Eng.* 129 (4): 296–306. https://doi.org/10.1061/(ASCE)1090-0241(2003)129:4(296).

Pan, X., J. Chu, Y. Yang, and L. Cheng. 2019. "A new biogrouting method for fine to coarse sand." *Acta Geotech.* 15 (1): 1–16. https://doi.org/10.1007/s11440-019-00872-0.

Polito, C. P., and J. R. Martin II. 2001. "Effects of nonplastic fines on the liquefaction resistance of sands." *J. Geotech. Geoenviron. Eng.* 127 (5): 408–415. https://doi.org/10.1061/(ASCE)1090-0241(2001)127:5(408).

Randolph, M. F. 2003. "Science and empiricism in pile foundation design." *Géotechnique* 53 (10): 847–875. https://doi.org/10.1680/geot.2003.53.10.847.

Rauthause, M. P., A. W. Stuedlein, and M. J. Olsen. 2020. "Quantification of surface roughness using laser scanning with application to the frictional resistance of sand-timber pile interfaces." *Geotech. Test. J.* 43 (4): 966–984. https://doi.org/10.1520/GTJ20180384.

Reddy, S. C., and A. W. Stuedlein. 2017. "Ultimate limit state reliability-based design of augered cast-in-place piles considering lower-bound capacities." *Can. Geotech. J.* 54 (12): 1693–1703. https://doi.org/10.1139/cgj-2016-0145.

Safavizadeh, S., B. M. Montoya, and M. A. Gabr. 2019. "Microbial induced calcium carbonate precipitation in coal ash." *Géotechnique* 69 (8): 727–740. https://doi.org/10.1680/jgeot.18.P.062.

Seo, H., I. Z. Yildirim, and M. Prezzi. 2009. "Assessment of the axial load response of an H pile driven in multilayered soil." *J. Geotech. Geoenviron. Eng.* 135 (12): 1789–1804. https://doi.org/10.1061/(ASCE)GT.1943-5606.0000156.

Spagnoli, G., P. Doherty, G. Murphy, and A. Attari. 2015. "Estimation of the compression and tension loads for a novel mixed-in-place offshore pile for oil and gas platforms in silica and calcareous sands." *J. Petrol. Sci. Eng.* 136 (Dec): 1–11. https://doi.org/10.1016/j.petrol.2015.10.032.

Stuedlein, A. W. 2008. "Bearing capacity and displacement of spread footings on aggregate pier reinforced clay." Ph.D. thesis, Dept. of Civil and Environmental Engineering, Univ. of Washington.

Stuedlein, A. W., W. J. Neely, and T. M. Gurtowski. 2012. "Reliability-based design of augered cast-in-place piles in granular soils." *J. Geotech. Geoenviron. Eng.* 138 (6): 709–717. https://doi.org/10.1061/(ASCE)GT.1943-5606.0000635.

Terzis, D., R. Bernier-Latmani, and L. Laloui. 2016. "Fabric characteristics and mechanical response of bio-improved sand to various treatment

conditions." *Geotech. Lett.* 6 (1): 50–57. https://doi.org/10.1680/jgele.15.00134.

van Paassen, L. A., C. M. Daza, M. Staal, D. Y. Sorokin, W. van der Zon, and M. C. M. van Loosdrecht. 2010a. "Potential soil reinforcement by biological denitrification." *Ecol. Eng.* 36 (2): 168–175. https://doi.org/10.1016/j.ecoleng.2009.03.026.

van Paassen, L. A., R. Ghose, T. J. M. van der Linden, W. R. L. van der Star, and M. C. M. van Loosdrecht. 2010b. "Quantifying biomediated ground improvement by ureolysis: Large-scale biogrout experiment." *J. Geotech. Geoenviron. Eng.* 136 (12): 1721–1728. https://doi.org/10.1061/(ASCE)GT.1943-5606.0000382.

Wang, Y., K. Soga, J. T. Dejong, and A. J. Kabla. 2019. "A microfluidic chip and its use in characterising the particle-scale behaviour of microbial-induced calcium carbonate precipitation (MICP)." *Géotechnique* 69 (12): 1086–1094. https://doi.org/10.1680/jgeot.18.P.031.

Whiffin, V. S. 2004. "Microbial $CaCO_3$ precipitation for the production of biocement." Ph.D. dissertation, School of Biological Sciences & Biotechnology, Morduch Univ.

Whiffin, V. S., L. A. van Paassen, and M. P. Harkes. 2007. "Microbial carbonate precipitation as a soil improvement technique." *Geomicrobiol. J.* 24 (5): 417–423. https://doi.org/10.1080/01490450701436505.

White, D. J., and M. D. Bolton. 2004. "Displacement and strain paths during plane-strain model pile installation in sand." *Géotechnique* 54 (6): 375–397. https://doi.org/10.1680/geot.2004.54.6.375.

Xiao, P., H. Liu, Y. Xiao, A. W. Stuedlein, and T. M. Evans. 2018. "Liquefaction resistance of bio-cemented calcareous sand." *Soil Dyn. Earthquake Eng.* 107 (Apr): 9–19. https://doi.org/10.1016/j.soildyn.2018.01.008.

Xiao, Y., H. Chen, A. W. Stuedlein, T. M. Evans, J. Chu, L. Cheng, N. Jiang, H. Lin, H. Liu, and H. M. Aboel-Naga. 2020. "Restraint of particle breakage by biotreatment method." *J. Geotech. Geoenviron. Eng.* 146 (11): 04020123. https://doi.org/10.1061/(ASCE)GT.1943-5606.0002384.

Xiao, Y., X. He, T. M. Evans, A. W. Stuedlein, and H. Liu. 2019a. "Unconfined compressive and splitting tensile strength of basalt fiber-reinforced biocemented sand." *J. Geotech. Geoenviron. Eng.* 145 (9): 04019048. https://doi.org/10.1061/(ASCE)GT.1943-5606.0002108.

Xiao, Y., L. Wang, X. Jiang, T. M. Evans, A. W. Stuedlein, and H. Liu. 2019b. "Acoustic emission and force drop in grain crushing of carbonate sands." *J. Geotech. Geoenviron. Eng.* 145 (9): 04019057. https://doi.org/10.1061/(ASCE)GT.1943-5606.0002141.

Xiao, Y., Z. Yuan, J. Chu, H. Liu, J. Huang, S. N. Luo, S. Wang, and J. Lin. 2019c. "Particle breakage and energy dissipation of carbonate sands under quasi-static and dynamic compression." *Acta Geotech.* 14 (6): 1741–1755. https://doi.org/10.1007/s11440-019-00790-1.

Xu, X., J. A. Schneider, and B. M. Lehane. 2008. "Cone penetration test (CPT) methods for end-bearing assessment of open- and closed-ended driven piles in siliceous sand." *Can. Geotech. J.* 45 (8): 1130–1141. https://doi.org/10.1139/T08-035.

Yasufuku, N., and A. F. L. Hyde. 1995. "Pile end-bearing capacity in crushable sands." *Géotechnique* 45 (4): 663–676. https://doi.org/10.1680/geot.1995.45.4.663.

Yasufuku, N., H. Ochiai, and S. Ohno. 2001. "Pile end-bearing capacity of sand related to soil compressibility." *Soils Found.* 41 (4): 59–71. https://doi.org/10.3208/sandf.41.4_59.

Yu, F. 2019. "Influence of particle breakage on behavior of coral sands in triaxial tests." *Int. J. Geomech.* 19 (12): 04019131. https://doi.org/10.1061/(ASCE)GM.1943-5622.0001524.

Zhang, C., G. D. Nguyen, and I. Einav. 2013. "The end-bearing capacity of piles penetrating into crushable soils." *Géotechnique* 63 (5): 341–354. https://doi.org/10.1680/geot.11.P.117.